Calmodulin extracts the Ras family protein RalA from lipid bilayers by engagement with two membrane-targeting motifs

Samuel G. Chamberlain[a,1], Andrea Gohlke[b], Arooj Shafiq[a,2], Iolo J. Squires[a,3], Darerca Owen[a,4], and Helen R. Mott[a,4]

[a]Department of Biochemistry, University of Cambridge, Cambridge CB2 1GA, United Kingdom; and [b]Mechanistic and Structural Biology, Discovery Sciences, R&D, AstraZeneca, Cambridge, CB4 0WG, United Kingdom

Edited by G. Marius Clore, NIH, Bethesda, MD, and approved August 5, 2021 (received for review March 7, 2021)

RalA is a small GTPase and a member of the Ras family. This molecular switch is activated downstream of Ras and is widely implicated in tumor formation and growth. Previous work has shown that the ubiquitous Ca^{2+}-sensor calmodulin (CaM) binds to small GTPases such as RalA and K-Ras4B, but a lack of structural information has obscured the functional consequences of these interactions. Here, we have investigated the binding of CaM to RalA and found that CaM interacts exclusively with the C terminus of RalA, which is lipidated with a prenyl group in vivo to aid membrane attachment. Biophysical and structural analyses show that the two RalA membrane-targeting motifs (the prenyl anchor and the polybasic motif) are engaged by distinct lobes of CaM and that CaM binding leads to removal of RalA from its membrane environment. The structure of this complex, along with a biophysical investigation into membrane removal, provides a framework with which to understand how CaM regulates the function of RalA and sheds light on the interaction of CaM with other small GTPases, including K-Ras4B.

membrane | K-Ras | calmodulin | Ral | nuclear magnetic resonance

RalA and RalB are members of the Ras superfamily of small GTPases, plasma membrane-associated molecular switches that regulate signal transduction affecting a plethora of cellular processes. Acting as one of the principal branches of the Ras signaling network, recruitment of a Ral-specific guanine exchange factor (RalGEF) promotes activation of RalA/B. Despite being less well studied than the MAPK and PI3K pathways, activation of RalGEFs is sufficient to induce Ras-driven transformation of human cells (1), and the inhibition of RalGEF disrupts colony formation in Ras-driven human cancer cell lines (2). It has also been reported previously that the RalGEF signaling pathway is crucial in the development of bone metastasis originating from pancreatic cancer in mice (3), and skin carcinoma mouse models deficient in RalGEF show decreased tumor size and number (4). Together, these findings indicate critical roles for both RalA and RalB in tumor formation and cancer progression, suggesting that it is important to expand our knowledge of their signaling roles and regulation.

RalA and RalB share 82% sequence identity in their G-domains (guanine nucleotide-binding domain) and are almost identical structurally (5). Both proteins contain two switch regions, the conformations of which are sensitive to the bound nucleotide, allowing downstream effectors to select the active form of the protein. The effector binding sequences of RalA/B are identical, and it is therefore surprising that they display functional divergence in vivo, mediating distinct cellular effects in both normal cells and in cancer settings (6–10). Most of the sequence diversity between the Ral isoforms comes from the aptly named hypervariable region (HVR) located at the C terminus. HVRs are short, intrinsically disordered regions found in all Ras and Rho family proteins, which have recently come under scrutiny for their ability to interact with membranes to regulate and modify signaling output of the G domain [reviewed by Cornish et al. (11)]. Some of the HVRs may have a propensity for secondary structure formation, such as the K-Ras4B HVR, which is α-helical under certain circumstances (12).

The C-terminal "CaaX box" motif (C = Cys, a = aliphatic, X = any residue) is the recognition sequence for isoprenylation of small GTPases, which facilitates their attachment to membranes. The C terminus of Ral proteins is recognized by GGTase-I (13), which adds a geranylgeranyl moiety to the Cys sidechain. The proteins are further processed by removal of the "aaX" motif and methylation of the new C-terminal carboxyl of the prenylcysteine (14). A secondary membrane attachment signal comes from positively charged Lys and Arg sidechains within the HVR, which interact with negatively charged phospholipid headgroups in the membrane bilayer. More than just a simple membrane anchor, the HVRs of RalA/B contain Ser residues that can be differentially phosphorylated in vivo. Ser194 of RalA is an Aurora kinase A target, phosphorylation of which has been shown to facilitate relocation to the mitochondrial membrane and binding to the effector RLIP76 (15).

Significance

RalA and RalB are membrane-attached small GTPases that are crucial for tumorigenesis and uncontrolled growth in Ras-driven cancers. The C-terminal tails of several Ras and Rho family small G proteins, which are lipidated in vivo, bind to the calcium sensor calmodulin. We have solved the structure of calmodulin in complex with the lipidated C-terminal tail of RalA and show that complex formation leads to RalA being removed from the lipid bilayer. We propose a mechanism for membrane removal of RalA, helping to shed light on the regulatory role that calmodulin plays in Ral signaling. This structure of a lipidated small G protein tail in complex with calmodulin may give clues about calmodulin interactions with other small G proteins, including K-Ras4B.

Author contributions: S.G.C., D.O., and H.R.M. designed research; S.G.C., A.G., and A.S. performed research; A.S. and I.J.S. contributed new reagents/analytic tools; S.G.C., A.G., D.O., and H.R.M. analyzed data; and S.G.C., A.G., D.O., and H.R.M. wrote the paper.

Competing interest statement: A.G. is an employee of AstraZeneca Ltd.

This article is a PNAS Direct Submission.

[1]Present address: Department of Biochemistry, University of Oxford, Oxford OX1 3QU, United Kingdom.

[2]Present address: Department of Biosciences, Salim Habib University, Karachi 74900, Pakistan.

[3]Present address: Biosciences Institute, Newcastle University, Newcastle upon Tyne NE2 4HH, United Kingdom.

[4]To whom correspondence may be addressed. Email: hrm28@cam.ac.uk or do202@cam.ac.uk.

This article contains supporting information online at https://www.pnas.org/lookup/suppl/doi:10.1073/pnas.2104219118/-/DCSupplemental.

Published September 3, 2021.

CaM (calmodulin) is a ubiquitous calcium sensor that regulates a multitude of partners. It is a small (16.7 kDa), pseudosymmetrical protein with two lobes (16), each comprising two EF-hand motifs. Upon calcium binding, the EF hands reorient to expose methionine-rich hydrophobic pockets that engage target proteins (17). The unusually high proportion of methionine residues, in conjunction with a flexible linker between the two lobes, confers extensive binding plasticity (18), allowing considerable sequence and structural diversity in CaM-interacting proteins. Binding often involves CaM wrapping around a positively charged helix in its target that contains hydrophobic anchors at defined positions in the sequence. These anchor residues dock into the hydrophobic pockets of the two CaM lobes. Alongside this canonical "wrap-around" mechanism, CaM also employs a variety of known noncanonical binding modes, which result in more extended conformations (19).

CaM has been shown to interact with the HVRs of RalA and RalB in a Ca^{2+}-dependent manner (19–21). It also binds the related small GTPase K-Ras4B in an interaction that involves burial of its C-terminal isoprenyl (farnesyl) group. Despite the interest in this interaction, there is no structure of K-Ras4B in complex with CaM. Although early data indicated that binding of K-Ras4B was nucleotide dependent, it is now thought that CaM binds to the prenylated C-terminal K-Ras4B HVR and that the nucleotide only controls accessibility of that region rather than binding directly to CaM (21). Biophysical data from one group indicated that two K-Ras4B molecules can bind to a single CaM, with the C-lobe of CaM binding around 10 times more tightly than the N-lobe (21). Another study used NMR titrations to show that the K-Ras4B protein is not necessary and that farnesyl compounds themselves are able to bind CaM (22). This was supported by a structure of a complex of CaM with farnesylated, methylated Cys, which binds exclusively to the C-lobe of CaM, in line with its higher affinity for that part of the CaM protein.

The interaction between RalA and CaM has not been studied as extensively, and there are conflicts in the literature as to the number of CaM-binding sites on Ral (20, 23) and the cellular consequences of the interaction. One study found that the interaction with CaM stimulated the GTPase "off-switch" of RalA (24), but another report showed that CaM binding caused RalA activation (20). Previous work has alluded to the importance of the prenyl anchor in the interaction (25), although there is a lack of biophysical data to corroborate and explain this observation. An in-depth structural and biophysical analysis of the RalA–CaM complex would allow an assessment of the potential functional consequences of this interaction. In this investigation, using maleimide-conjugated prenyl mimics, we sought to elucidate the molecular basis for the interaction between RalA and CaM to better understand its role in vivo. We establish that the binding motif for CaM is within the RalA-HVR and demonstrate the importance of the prenyl anchor for high affinity binding. We have solved the first structure of CaM in complex with a lipid-modified HVR, which shows that the N-lobe of CaM encases the prenyl group whereas the C-lobe interacts with key hydrophobic residues of the HVR. Furthermore, we show that CaM is able to extract RalA from the surface of a lipid membrane and propose a stepwise temporal order for the mechanism. Other small GTPases suspected of interaction with CaM, such as RalB, Rac1, Cdc42 (26), and Rap1A (27), have features in common with RalA, including a polybasic motif and prenyl moieties at their C termini. The results presented here may therefore provide a framework to understand the interaction of CaM with these proteins.

Results

A 10-Residue C-Terminal Motif Defines the Core CaM-Binding Site of RalA. An 18-residue fragment of the RalA C terminus (SKEK NGKKKRKSLAKRIR) was described as the putative CaM-binding site (23, 24, 28), based on sequence inspection and the assumption that the binding motif must contain an amphipathic helix (23). It has also been suggested that there is a second CaM-binding site within the disordered N-terminal extension of RalA (20). To unambiguously define the CaM-binding site on RalA, we carried out NMR-based chemical shift perturbation (CSP) experiments (Fig. 1*A* and *SI Appendix*, Fig. S1*A*) in the presence of Ca^{2+}, utilizing ^{1}H-^{15}N heteronuclear single quantum correlation (HSQC) experiments recorded on ^{15}N-labeled RalA·GMPPNP missing the last three residues (CΔ3, reference *SI Appendix*, Table S1). The majority of resonances in the RalA spectrum exhibited no change when unlabeled CaM was added, indicating that they are not involved in the interaction, and the N terminus and G domain were relatively unperturbed (CSP less than 0.02 ppm). The resonances corresponding to HVR residues 179 to 193, just C-terminal to the G domain, shifted upon CaM binding, but the changes were rather small (less than 0.03 ppm), and their positions could be followed during the course of the titration. The C-terminal Cys203 shifted significantly (CSP 0.19 ppm), but its position could also be tracked during the titrations (*SI Appendix*, Fig. S1*A*). In contrast, resonances corresponding to residues 194 to 202 of the HVR (SLAKRIRER) disappeared during the titration and gradually reappeared at different positions as the titration progressed. This is known as slow exchange and indicates that the chemical shift differences between the free and CaM-bound states for these resonances are larger than the rate of exchange between these states. Such behavior demonstrates that these residues are involved in binding CaM, and the slow exchange rate between free and bound states strongly suggests that it is a high affinity interaction.

The role of the C terminus of RalA in CaM binding was confirmed using scintillation proximity assays (SPA), where [^{3}H]GTP·RalA was titrated into His-tagged CaM immobilized on an SPA bead (*SI Appendix*, Fig. S1*B*). Full-length RalA (*SI Appendix*, Table S1) bound to both CaM and to the Ral effector RLIP76, whereas a construct truncated at the end of G domain (CΔ21) only bound to RLIP76. The interaction of full-length RalA with CaM was also Ca^{2+} dependent, since addition of the Ca^{2+}-chelator EGTA abrogated the binding (*SI Appendix*, Fig. S1*B*). All subsequent experiments were therefore performed in the presence of Ca^{2+}.

Overall, this analysis indicates that there is only one CaM-binding site in RalA, the core motif of which corresponds to 10 residues at the C terminus of the HVR.

RalA Interaction with CaM Is Increased by Its Prenylation but Is Independent of Nucleotide Status or Ser194 Phosphorylation. Isothermal titration calorimetry experiments (ITC) were used to measure the affinity and stoichiometry of the interaction between CaM and RalA. Titrating CaM into full-length RalA, which includes the three extra C-terminal hydrophobic residues, resulted in an isotherm that yielded a K_d of 0.5 μM and a 1:1 stoichiometry (Fig. 1*B* and *SI Appendix*, Table S2). In vivo, Cys203 is the site of modification with geranylgeranyl, and the three C-terminal residues are removed. Although the interaction between CaM and RalA CΔ3 was observed by NMR (Fig. 1*A*), only small heat changes were observed during the titration of CaM into RalA CΔ3, which could not be fit to the isotherm (Fig. 1*B*). We therefore tested the effect of a lipid prenyl moiety at Cys203 by using maleimide chemistry to modify the Cys sidechain. To achieve specific labeling of only the C-terminal Cys sidechain, the only other Cys in RalA, Cys91, was substituted with Ala. We synthesized two maleimide-functionalized prenyl anchor mimics (*SI Appendix*, Fig. S2*A*), MFn (maleimido-farnesyl), which includes a 15-carbon farnesyl group, and MGG (maleimido-geranylgeranyl), which includes a 20-carbon geranylgeranyl. RalA CΔ3 prenylated with MGG was insoluble in the absence of detergents but could be stabilized by binding to nanodisc membrane mimics. Titration of CaM into nanodisc-bound RalA CΔ3 MGG resulted in a return of heat

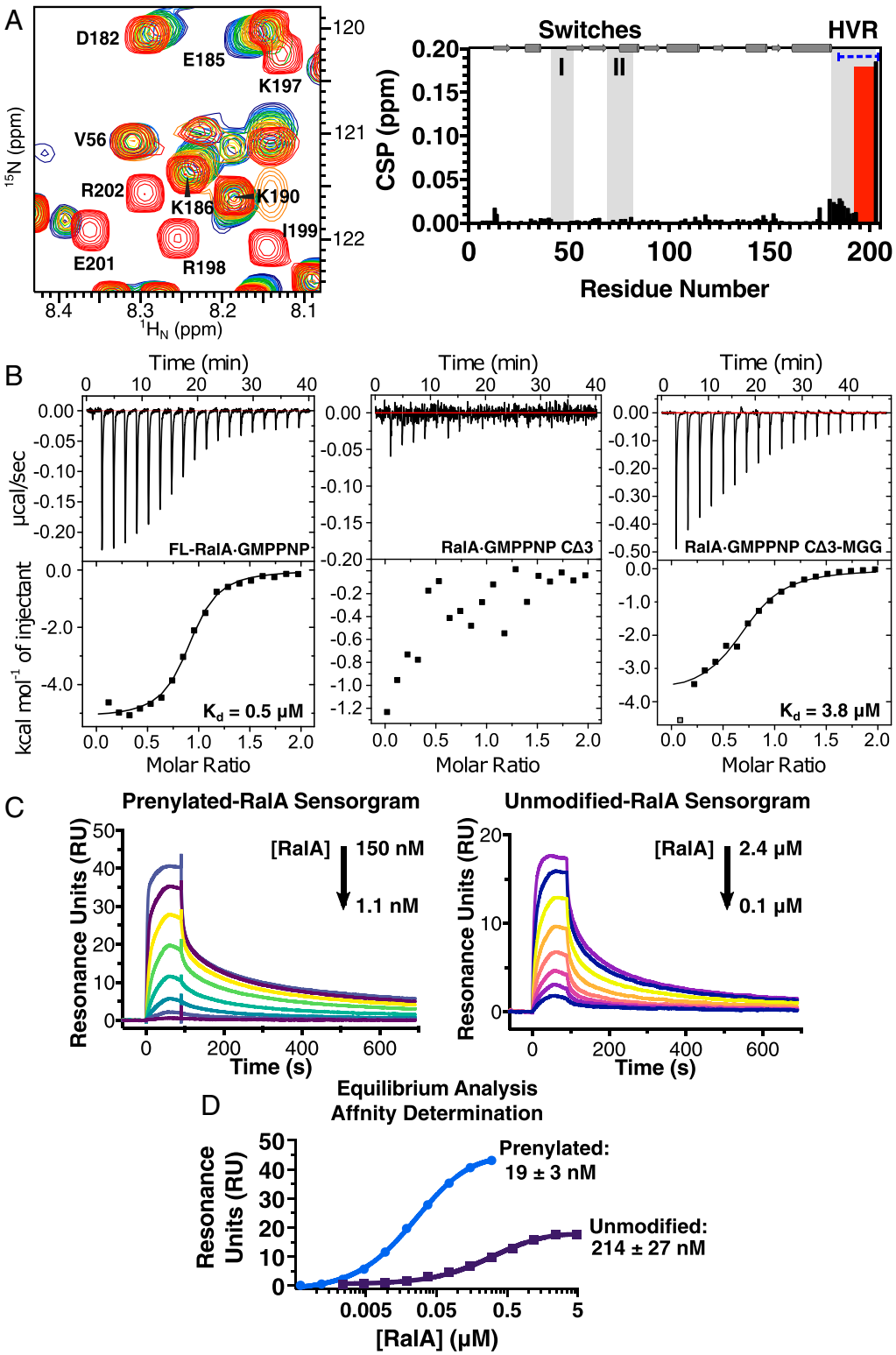

Fig. 1. Defining the CaM-binding site in RalA. (*A*, *Left*) ^{1}H-^{15}N HSQC spectra of ^{15}N-labeled RalA CΔ3 in the absence (red) and presence of 0.25 (orange), 0.5 (yellow), 0.75 (green), 1 (blue), and 1.5 (violet) molar equivalents of CaM. The region of the HSQC shows resonances that do not move during the titration (e.g., Val56), those that remain close to their original position (e.g., Asp182 and Glu185), and those that have shifted too far to reliably track (e.g., Arg202 and Ile199). (*Right*) Quantification of the CSP between the first and last point in the titration versus residue number. The red bars indicate residues that shifted too far during the titration for reliable assignment. The secondary structural elements are indicated by arrows (β-strands) and cylinders (α-helices). The nucleotide-sensitive switch regions and the HVR residues are shaded in gray. The blue dashed line indicates the location of the peptide used in later experiments. (*B*) ITC experiments with RalA GMPPNP constructs. CaM was titrated into either (*Left*) FL-RalA·GMPPNP (including the CIL of the CaaX box), (*Middle*) RalA·GMPPNPCΔ3, or (*Right*) RalA·GMPPNP CΔ3 lipidated with MGG, in the presence of nanodiscs. (*C*) Representative sensorgrams from the SPR experiments with prenylated (MFn) and unmodified RalA CΔ3. (*D*) Affinities from equilibrium analysis calculated over multiple independent repeats (n = 6 and 5) are shown as mean ± SE.

changes and an apparent binding affinity of 3.8 μM (Fig. 1*B*). These data indicate that enthalpically productive encounters can only occur in the presence of a hydrophobic moiety at the C terminus of RalA. Although they are not present in the native, processed protein, we reasoned that the extra hydrophobic residues in full-length RalA could be partially mimicking the effect of prenylation. Furthermore, the reduced affinity in the presence of nanodiscs suggests that there is competition between CaM and the membrane for binding of the geranylgeranyl group.

The binding of prenylated RalA to CaM was further explored using surface plasmon resonance (SPR). Here, the protein was modified with farnesyl, which renders it more soluble without detergents. The overall length of MFn is closer to that of the native geranylgeranyl modification than MGG (*SI Appendix*, Fig. S2*B*), although it is less hydrophobic. CaM was immobilized on the surface of a CM5 sensor chip via amine coupling and multicycle experiments recorded by flowing either RalA CΔ3 or RalA CΔ3-MFn over the immobilized protein (Fig. 1*C*). Dissociation constants for unmodified and prenylated RalA calculated by 1:1 equilibrium analysis (Fig. 1*D*) were 214 ± 27 nM and 19 ± 3 nM, respectively. Hence, modification of RalA with MFn appears to increase the affinity for CaM ∼10-fold. The K_d of RalA CΔ3 MGG and CaM measured by SPR was 45 nM (*SI Appendix*, Fig. S3), so this modification increases the affinity around fivefold compared with the nonprenylated RalA.

We then asked whether the interaction between RalA and Cam is modulated by the nucleotide bound to RalA or by Aurora A phosphorylation at Ser194, which occurs within the 10 residue CaM-binding site. ITC experiments were used to investigate whether the RalA–CaM interaction can still occur when RalA is GDP-bound or when it is mutated to Asp at Ser194, which has been shown to be a reliable phosphomimic in a cell-based setting (15). RalA·GDP-MGG and the S194D RalA·GMPPNP-MGG attached to nanodiscs both interacted with CaM with a similar affinity to that of RalA·GMPPNP-MGG (*SI Appendix*, Fig. S4 and Table S2) and, importantly, could bind in the context of a membrane environment. Interestingly, the S194D mutation, despite having little effect on the overall affinity, showed very different thermodynamic parameters, with much larger heat changes that were offset by an unfavorable entropic term. This is presumably due to differences in the interactions between Ser194/Asp194 and the membrane lipid headgroups.

The Prenyl Anchor Is Necessary to Engage Both Lobes of CaM and Lead to Their Reorientation. MFn-modified RalA was used in NMR experiments due to its higher solubility and similar length to geranylgeranyl (*SI Appendix*, Fig. S2). To further explore how the prenyl anchor of RalA confers an increase in affinity to CaM, we carried out NMR experiments, where either RalA·GMPPNP CΔ3 (nonlipidated) or RalA·GMPPNP CΔ3-MFn were titrated into ^{15}N-labeled CaM and ^{1}H-^{15}N HSQC experiments recorded (Fig. 2*A*). Titration of RalA CΔ3 into CaM resulted in only small changes within the N-lobe and central linker of CaM but larger and more widespread changes in the C-lobe (Fig. 2). This suggests that the C-lobe makes most of the contacts with RalA CΔ3. In comparison, titration of RalA CΔ3-MFn into CaM resulted in more substantial changes that extended throughout both lobes of CaM, and in some cases the resonances had shifted too far to be reliably assigned. Furthermore, resonances in the acidic central linker (Fig. 2*B*) were also affected. Taken together, these NMR titrations indicate that the C-lobe engages the HVR, which is present in RalA CΔ3, whereas the prenyl anchor is sequestered by the hydrophobic pocket of the N-lobe when RalA CΔ3-MFn is added. The changes in the CaM chemical shifts, as well as extending over more of the protein, were larger in size in the complex with prenylated RalA. This, along with the involvement of the flexible central linker, indicates that CaM undergoes a conformational rearrangement upon binding to RalA CΔ3-MFn. Conformational changes are often observed in CaM when it binds to its targets and can involve melting of the central helix and reorientation of the lobes (Fig. 2*A*). Strikingly, this extensive rearrangement only occurs when binding RalA in the presence of the prenyl anchor.

The Structure of the Prenylated RalA HVR–CaM Complex. The NMR titrations showed that a 10-residue motif of the RalA-HVR engages with the C-lobe of CaM (Figs. 1*A* and 2). A peptide based on the RalA-HVR (residues 187 to 203), including this binding motif, was titrated into ^{15}N-labeled CaM, and HSQC spectra showed a similar pattern and extent of changes as with the titration of the RalA CΔ3 protein (*SI Appendix*, Fig. S5). This indicates that the binding of the HVR peptide recapitulates the binding of RalA. Uniformly ^{13}C,^{15}N-labeled, HVR peptide was expressed in *Escherichia coli* and lipidated with MFn. NMR titrations of unlabeled CaM into the labeled peptide showed that residues within the core 10-residue motif were most affected (*SI Appendix*, Fig. S6). Attempts to obtain a crystal structure of the CaM–HVR–MFn complex were unsuccessful; therefore, we used NMR to solve the structure (Fig. 3). The resonances were assigned using standard triple resonance backbone and sidechain experiments. The farnesyl moiety was assigned using two-dimensional (2D) spectra of the free peptide and 2D isotope-filtered experiments of the complex of labeled CaM with unlabeled peptide (29, 30). The structure was calculated using distance restraints derived from a variety of NOESY (nuclear Overhauser effect spectroscopy) experiments (*SI Appendix*, *Supplementary Materials and Methods*), including 3D ^{15}N,^{13}C-filtered, ^{13}C-separated NOESY experiments for intermolecular distance restraints (*SI Appendix*, Fig. S7 and Table S3). A total of 40 NOEs between the farnesyl moiety and CaM were observed, as well as 82 NOEs between CaM and the HVR.

This represents the first structure of a lipidated small GTPase HVR in complex with CaM, and the total buried surface area of the complex is 1,200 Å^2 [calculated with Proteins, Interfaces, Structures and Assemblies (PISA) at the European Protein Data Bank (PDBe) (31)]. The N-terminal portion of the HVR remains disordered in the complex, as predicted by our NMR titrations (Fig. 1*A* and *SI Appendix*, Figs. S1 and S6). Upon interaction with the RalA-HVR, the central helix of CaM undergoes extensive unfolding between residues Lys75 and Glu84. Melting of this helix to this extent, although uncommon in CaM structures, is consistent with previous observations that helical content decreases upon complex formation with the RalA HVR (23). This unfolded linker, coupled with the partial disorder of the HVR, results in the lack of fixed orientation of the N-lobe with respect to the C-lobe (Fig. 3*A*). There is a notable absence of interlobe NOEs, and residues of the central linker show only short-range, mostly intraresidue NOEs, which are not indicative of secondary structure.

The N-lobe of CaM sequesters the prenyl anchor via extensive interactions within a deep cavity lined with hydrophobic aliphatic and aromatic sidechains of residues in both EF-hand motifs (Fig. 3 *C* and *D* and *SI Appendix*, Fig. S8*A*). Ala15 and Leu32 at the mouth of the pocket are on either side of the propionate ester linking the farnesyl with the maleimide group and are small enough to allow the farnesyl group to enter the cavity. The first part of the pocket is lined by two pairs of Met sidechains, whose flexibility allows them to rearrange around the isoprenyl. Two Phe sidechains (19 and 68) on one side of the pocket fill up the space as the tetrahedral carbon of C5 changes the direction of the farnesyl group toward the other side of the pocket. Deep within the pocket, the two methyl groups at the end of the farnesyl are packed against the methyl groups of four methyl-containing sidechains: Ile27, Leu32, Val55, and Ile63.

The N terminus of the HVR is extended, with residues 186 to 191 having no NOEs to CaM, consistent with the NMR titrations that showed that their resonances were relatively unperturbed when CaM was added (Fig. 1 and *SI Appendix*, Fig. S6). NOEs were observed between Arg192 and Lys193 and residues in the linker between the two EF hands of the C-lobe. Ser194 is solvent

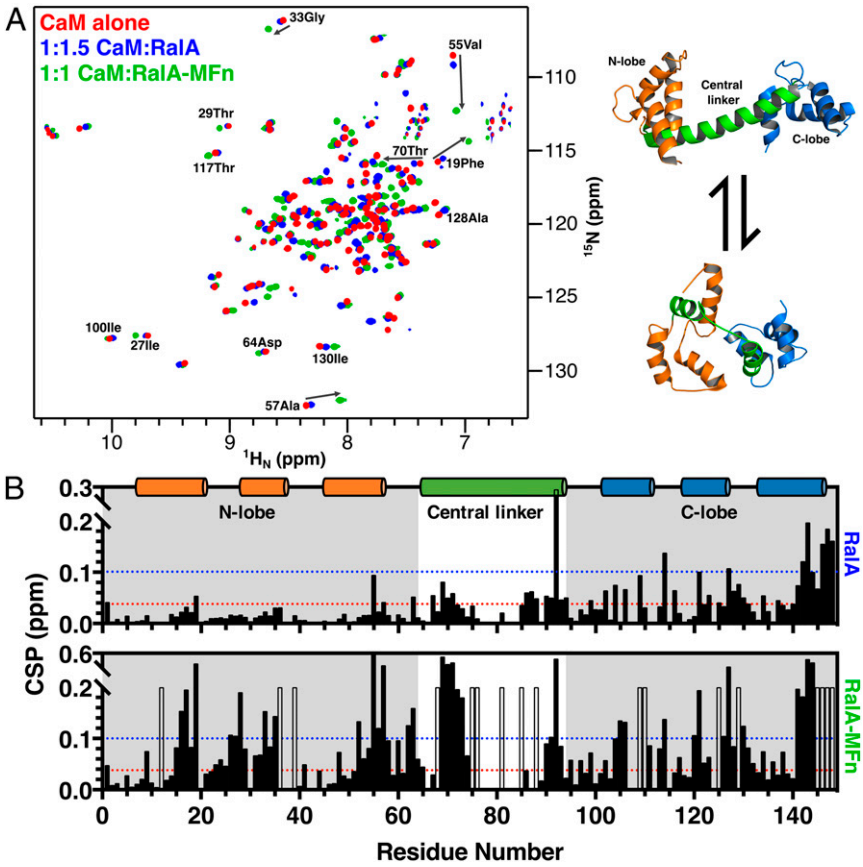

Fig. 2. The binding surface of CaM responsible for interaction with RalA. (*A*, *Left*) ^{1}H-^{15}N HSQC spectra of ^{15}N-labeled CaM alone (red) and in the presence of 1.5 molar equivalents of RalA CΔ3 (blue) or one molar equivalent of RalA CΔ3 with a covalently linked farnesyl (MFn) anchor (green). Arrows show selected resonances that differ when titrating in RalA with/without the farnesyl anchor. (*Right*) Schematic to show the conformational rearrangement in CaM upon canonical wrap-around binding to its targets. The N-lobe is orange, the central helix is green, and the C-lobe is blue. Structures are PDB accession codes 1CLL (*Upper*) and 1IQ5 (*Lower*). (*B*) Quantification of the CSP for the titration experiments. Solid bars represent quantifiable shift changes; hollow bars represent residues whose final peak position is unknown due to their large shift perturbation. Average CSPs for titration with RalA CΔ3 and RalA CΔ3-MFn are shown as red and blue dotted lines, respectively. The secondary structure of CaM is shown above the graph, with the helices represented as cylinders and the regions of CaM colored as in *A*.

exposed, and this is followed by Leu195, then a single turn of α-helix between Ala196 and Arg200. This helix is not present in the free peptide but in the complex, it is stabilized by the projection of two hydrophobic residues, Leu195 and Ile199, into two shallow hydrophobic pockets in the CaM C-lobe. Here, Leu195 forms hydrophobic interactions with residues Leu105, Met109, Leu116, Met124, and Met145, while Ile199 contacts the CaM residues Ile85, Ala88, Phe92, and Phe141 (*SI Appendix*, Fig. S8*B*). The HVR helix is further stabilized by electrostatic interactions that can form between Glu201 and Lys197 or Arg198. Electrostatic interactions on either side of this short helix also contribute to the binding of the complex (*SI Appendix*, Fig. S8*B*), although they are generally formed between regions whose structures are not well-defined and therefore are variable in the different members of the ensemble. The HVR Arg192 can form salt bridges with Glu120 and Glu123 in the CaM C-lobe, and the Lys residues on either side of this Arg also contact acidic residues in the C-lobe, particularly Lys191 to helix α7 (Glu120, Glu123, and Glu127), Lys193 to helix a7, and Glu114 in the α6-α7 loop. On the other side of the HVR helix, Arg200 can contact Asp78 and Asp80 in the CaM interlobe linker, and Arg202 interacts predominantly with Asp80 but can also contact Glu82 and Glu84.

To understand the role of the hydrophobic interactions between the HVR and the C-lobe, a RalA construct was generated where both HVR residues were substituted with Ala. NMR titrations showed that CSPs were completely ablated when the L195A I199A variant RalA was used (*SI Appendix*, Fig. S9).

To assess whether the structure presented here is a good mimic of the native geranylgeranylated HVR of RalA in vivo, we recalculated the structure using the same distance restraints but applied to Cys-geranylgeranyl (GG) instead of the Cys-MFn prenyl-mimic (*SI Appendix*, Fig. S10). The resulting structure showed that GG can be accommodated in the malleable CaM N-lobe hydrophobic pocket (RMSD of the N-lobe backbone is 0.57 Å), and the total buried surface area of the complexes with the MFn and GG lipidated HVR are 1,200 Å^2 and 1,297 Å^2, respectively [PDBePISA (31)].

RalA Is Removed from Membranes by CaM. Our structural and biophysical analysis showed that the interaction between RalA and CaM is driven by the HVR of RalA and that there is no interaction with the G domain. This raised the question of the function of this interaction in vivo. Previous work has shown that the related GTPase K-Ras4B is removed from the plasma membrane by CaM (21, 22, 27, 32). We therefore assessed whether RalA could be similarly extracted from a membrane. RalA·GMPPNP CΔ3-MGG attached to nanodiscs was pulled down onto Ni^{2+} beads using the His-tag on the MSP1D1 nanodisc belt protein. The beads were washed with either CaM

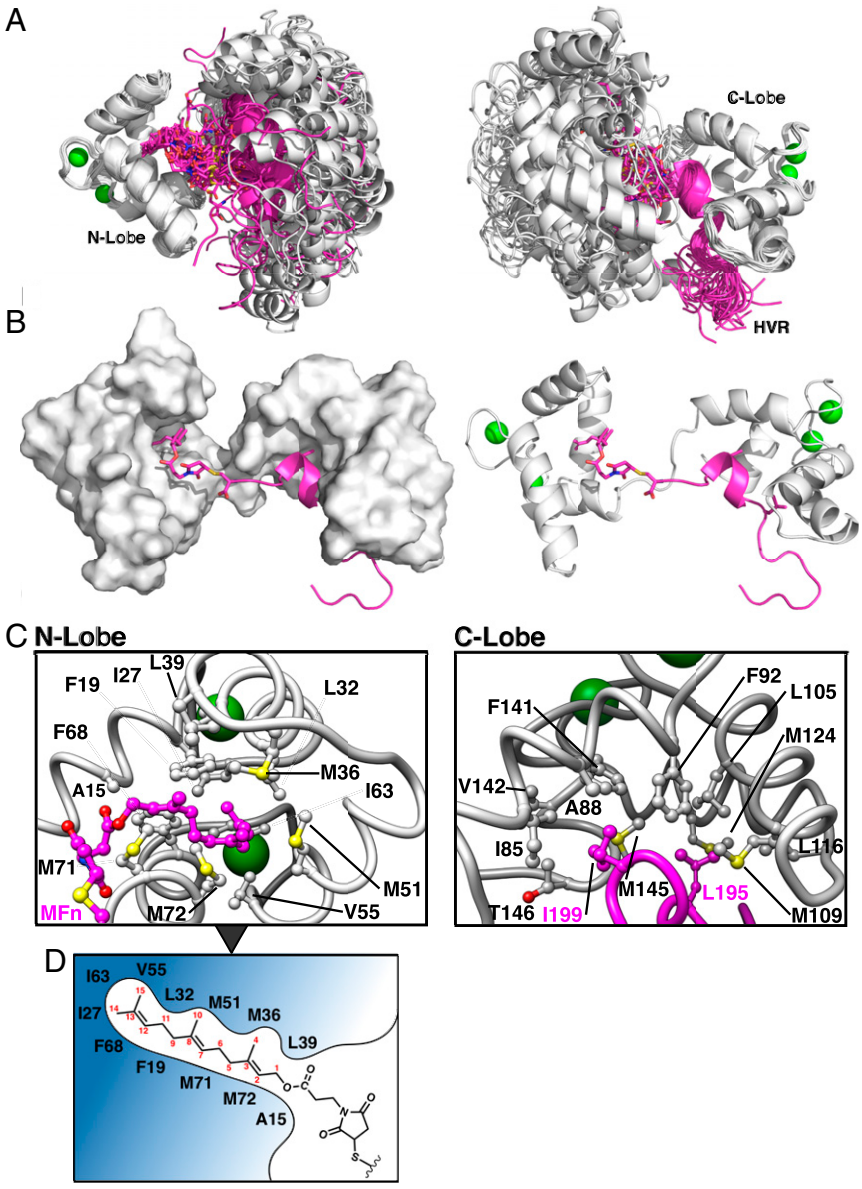

Fig. 3. NMR structure of lipidated RalA-HVR peptide in complex with CaM. (*A*) Superimposition of the 40 lowest energy calculated structures, overlaid using either the N-lobe (*Left*) or C-lobe (*Right*) of CaM. CaM is gray with Ca^{2+} represented by green spheres. The HVR is magenta with a stick representation for the MFn. The PDB accession code is 7NQC. (*B*) Closest to the mean structure. Color scheme as above. (*Left*) Surface representation and (*Right*) cartoon of CaM showing the hydrophobic cavity of the N-lobe that accommodates the prenyl lipid and the shallow hydrophobic pockets formed by the C-lobe to accommodate the hydrophobic module of the HVR (Leu195 and Ile199, sticks). (*C*) Detailed views of the N-lobe and C-lobe hydrophobic pockets. Interfacial residues are shown as balls and sticks and are colored as follows: carbon (gray for CaM, magenta for RalA), nitrogen (blue), oxygen (red), and sulfur (yellow). (*D*) Schematic of the amino acids lining the prenyl binding pocket, carbon atoms in MFn are numbered.

or buffer and probed by Western blot (Fig. 4*A*). RalA was retained on the nanodiscs when they were washed with buffer but was eluted by CaM.

In an orthogonal assay, SPR was used to probe whether CaM could remove RalA from a membrane. Liposomes were immobilized to form a supported bilayer/tethered liposome surface. As RalA-MGG is insoluble in the absence of detergent, we flowed the more stable RalA CΔ3-MFn over the membrane surface, which was washed to achieve a stable baseline. As CaM was subsequently washed over the sensor, the signal decreased as RalA was removed from the surface of the membrane (Fig. 4*B*). The decrease in signal after CaM injection was typically ∼20% of the total signal. This partial removal suggests that not all of the RalA is accessible in this experimental setup, presumably CaM removes RalA mainly from the solvent-exposed top face, but the Ral protein can bind other regions of the liposomes that are more occluded. Similar experiments performed on K-Ras4B also showed only partial removal (33). In contrast, the RalA L195A I199A CΔ3-MFn variant protein could not be removed from supported liposomes by CaM (Fig. 4*B*). Along with validating the structure, this shows the critical role played by these hydrophobic residues in the capture of the HVR by the C-lobe of CaM and the importance of this capture in the mechanism of membrane removal.

RalB Has a Lower Affinity for CaM. The work presented here focuses on the RalA–CaM interaction, however it has been reported that both isoforms of Ral can interact with CaM (20, 25). Given the sequence variability between the C termini of

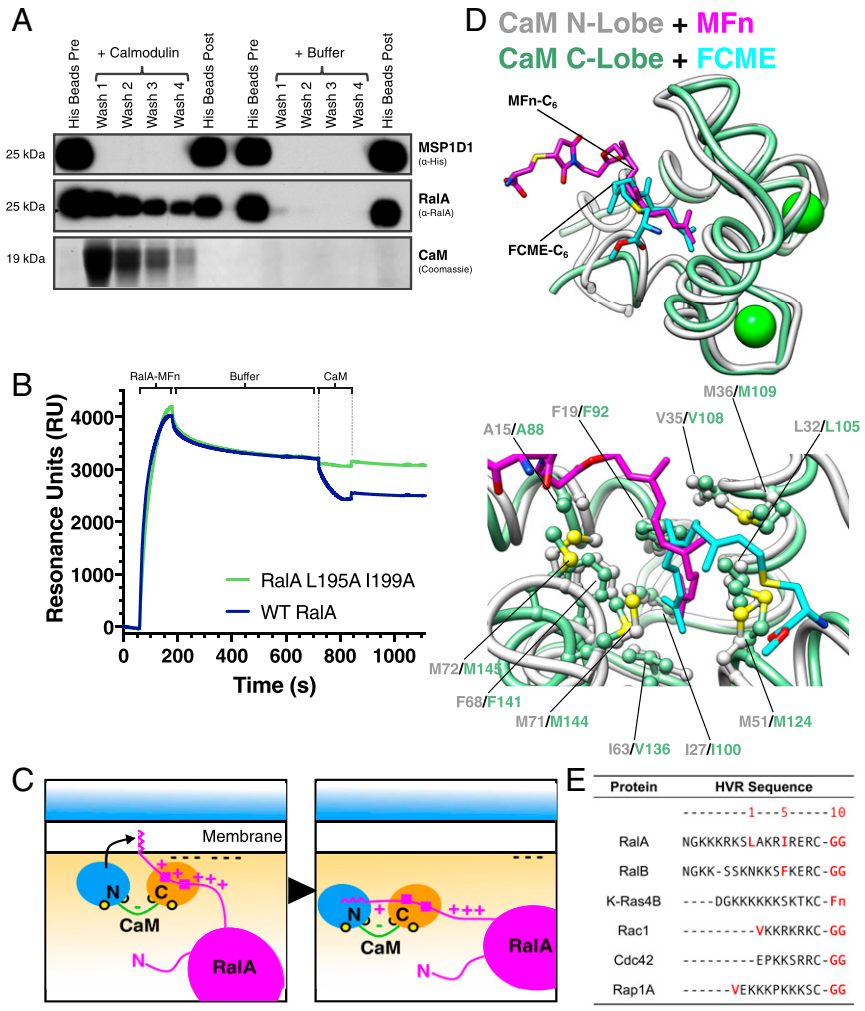

Fig. 4. CaM extracts RalA from membranes. (*A*) RalA-MGG bound to nanodiscs was pulled down onto Ni^{2+}-NTA by the His-tag on the MSP1D1 nanodisc scaffolding protein. The beads were either incubated with CaM (*Left*) or buffer (*Right*). RalA was eluted in complex with CaM but not by buffer. (*B*) Representative sensorgrams from SPR experiments using 10% PS-containing liposomes supported on the surface of an L1-chip. RalA-MFn (blue) or RalA L195A I199A-MFn (green) were flowed over the chip to load RalA onto the membrane, followed by a buffer wash to achieve a stable baseline. CaM was then flowed over, and a decrease in RU corresponding to removal of RalA was observed with wild-type (WT) RalA but not the L195A I199A double mutant. (*C*) The proposed mechanism of RalA removal from a membrane. (*Top*) A two step mechanism of membrane removal. (*Left*) The C-lobe of CaM (orange) competes with the membrane for interaction with the HVR of RalA (magenta). Positive charges of the secondary membrane-targeting sequence and negative phospholipids of the inner leaflet of the PM are shown as + and −, respectively. The Ca^{2+}-loaded C-lobe of CaM (orange) first grips the hydrophobic residues of the RalA HVR (magenta squares). Flexibility of the central linker region (green) allows the capture and removal of the prenyl anchor. (*Right*) Burial of the prenyl anchor in the N-lobe (blue) of CaM allows the solubilization and extraction of RalA from the membrane. (*D*) A superimposition of MFn (magenta) binding to the N-lobe of CaM (gray, our structure) and FCME (cyan) with the C-lobe of CaM (green, PDB: 6OS4). (*Upper*) An overview of the two structures; (*Lower*) the prenyl binding pockets with key hydrophobic residues, labeled and shown in ball and stick representation. (*E*) Sequences of various GTPases known to interact with CaM aligned via their C-terminal prenyl lipid moiety. Hydrophobic residues are colored red.

RalA and RalB (Fig. 4*D*), there are likely to be differences in their interaction with CaM. A peptide representing the HVR of RalB was titrated into ^{15}N-labeled CaM (*SI Appendix*, Fig. S11) and ^{15}N HSQC experiments were recorded. Addition of the RalB HVR peptide elicited changes in the central linker and in the C-lobe of CaM. Compared with the effects of titration of the RalA HVR peptide, however, the changes were much smaller (*SI Appendix*, Fig. S11*A*), resulting in a fourfold smaller average CSP (*SI Appendix*, Fig. S11*B*). This indicates that the CaM–RalA binding interface is more extensive than that of CaM–RalB, suggesting that RalA binds more tightly. To corroborate this, SPR experiments were performed to determine the affinities of RalB-MFn and CaM (*SI Appendix*, Fig. S12). The interaction of CaM with RalB-MFn was shown to have an affinity of 95 nM, fivefold weaker than that with RalA-MFn (19 nM, Fig. 1*C*).

Discussion

The interaction between RalA and CaM, although widely reported, has thus far only been superficially characterized biophysically, leading to an inability to assess the conflicting evidence as to the function of this complex. Here, we have carried out a detailed structural and biophysical investigation of the RalA–CaM complex and its functional consequences.

Interactions with CaM often involve the formation of amphipathic helices with hydrophobic anchor residues at defined positions in the sequence, whose spacing defines the mode of CaM interaction (reviewed in ref. 19). Sequence analysis of the RalA C terminus led to the assumption that RalA would conform to the canonical "wrap-around" CaM interaction, with the RalA-HVR forming an extensive amphipathic helix, despite CD evidence to the contrary (23). It is widely accepted that the HVRs

of Ras superfamily GTPases are intrinsically disordered, even in the context of the membrane, and indeed, it is thought that this disorder is crucial to their function and regulation (11). This structure shows that the RalA-HVR forms only a single helical turn, remaining mainly disordered even when in complex with CaM. There is no involvement of the RalA G domain in the interaction (Fig. 1*A* and *SI Appendix*, Fig. S1), and the interaction of CaM with RalA CΔ3 and the HVR peptide is almost identical (*SI Appendix*, Fig. S5). The HVR of RalA displays marked specificity for the C-lobe of CaM (Fig. 2) despite the overall similarity of the two lobes of CaM. This inability for the HVR to bind the N-lobe explains the reduced surface activity that we observed in the SPR experiments involving unmodified RalA when compared to lipidated RalA. The latter can bind to either CaM lobe, whereas unmodified RalA can only bind to those CaM molecules whose C-lobe is accessible, assuming random CaM orientation on the amine-reactive chip.

The partially disordered HVR peptide in this complex, combined with flexibility in the orientations of the N- and C-lobes, is an unusual mode of CaM interaction, and there are only two other CaM-complex structures with this conformational flexibility: Munc13-1-CaM (34) and the MA-domain$^{\text{HIV-1 Gag}}$ -CaM (35). All of these CaM-binding motifs are characterized by the presence of two hydrophobic modules separated by a flexible linker region, resulting in the extended CaM-binding mode (*SI Appendix*, Fig. S13). Similarity can also be drawn with the Myelin Basic Protein (MBP) complex, where the two lobes of CaM remained flexible in the complex (36). Like RalA, the CaM-binding motifs of both MBP and HIV-1 Gag are within regions that bind membranes. CaM is involved in dissociation of MBP from the membrane whereas the interaction between HIV-1 Gag and CaM has been suggested to play a role in both delivery and release from the plasma membrane (37).

The structural data for the RalA HVR–CaM complex allows the assessment of possible or likely functions of this interaction, of which there have been conflicting ideas (20, 24). We have shown that CaM removes RalA from a membrane (Fig. 4 *A* and *B*) and that Leu195 and Ile199 are essential for interactions with the CaM C-lobe (*SI Appendix*, Fig. S9). The affinity of geranylgeranylated RalA for CaM in the absence of a membrane is 45 nM by SPR (*SI Appendix*, Fig. S3), but when nanodiscs were present the apparent affinity was reduced ∼80-fold, although this was measured by ITC (Fig. 1*B*). ITC experiments showed that the affinity of full-length RalA for CaM is 7.5 times higher than that of MGG-modified RalA on nanodiscs (Fig. 1*B*). Hence, there is likely to be competition for the HVR between the membrane and the C-lobe of CaM. The observation that the L195A, I199A double mutant blocks removal of RalA from the membrane surface (Fig. 4*B*) suggests that these interactions are crucial for the mechanism of membrane removal and allows a model to be proposed (Fig. 4*C*). RalA is attached to the membrane via its geranylgeranyl anchor and basic residues in the HVR interacting with anionic phospholipids. To remove RalA, the C-lobe of CaM first competes with the membrane surface for interaction with the basic HVR. There are four Arg and two Lys residues in the CaM-binding region, so it is likely that these are part of the membrane-binding basic patch. CaM engages the Leu/Ile hydrophobic motif, stabilized by salt bridges formed between the Arg/Lys residues of the HVR and the central linker and α7 of the C-lobe. After the C-lobe disrupts HVR–membrane interactions, reorientation of the CaM lobes then allows the withdrawal and capture of the prenyl anchor from the membrane. A question remaining is how this process is controlled, apart from by local Ca^{2+} concentrations, and one possibility is via the phosphorylation of RalA Ser194. We have shown that the phosphomimic RalA S194D attached to nanodiscs can still bind to CaM (*SI Appendix*, Fig. S4), and the structure shows that the sidechain of Ser194 does not make significant contacts with CaM (*SI Appendix*, Fig. S14) so that its phosphorylation would not affect the interaction of the hydrophobic anchor residues. Interestingly, the thermodynamics of the interaction between S194D RalA and CaM was not the same as that between nanodisc-bound wild-type RalA and CaM. Our interpretation of this is that the addition of the negative charge at position 194 changes the orientation of RalA at the membrane. This may make it more accessible to the solvent, which could explain the different enthalpic contribution when S194D binds to CaM. This would also make it easier for the C-lobe of CaM to engage the RalA HVR and remove RalA from anionic membranes.

Other small GTPases of the Ras superfamily have been shown to interact with CaM, including K-Ras4B (38), Rac1, Cdc42 (26), and Rap1A (27). The best studied is the K-Ras4B–CaM interaction, which can be compared with the Ral–CaM complexes. The binding of K-Ras4B is clearly not as strong as that of the RalA HVR: unmodified RalA CΔ3 binds to CaM with an affinity of ∼200 nM, and lipidation of RalA increases the affinity 10-fold. In contrast, the unmodifed K-Ras4B bound with an affinity of 3 μM (39), which again increased 10-fold to 400 nM for fully processed K-Ras4B (21). The very different affinities of RalA and K-Ras4B are reflected in the NMR titrations of the two proteins into labeled CaM. Titrating either unmodified RalA CΔ3 or the equivalent HVR peptide into ^{15}N-labeled CaM leads to changes in the C-lobe of CaM (Fig. 2 and *SI Appendix*, Fig. S5), but the same experiment with unmodified K-Ras4B produced no (21) or very small shift changes (22) in CaM. When a peptide representing the K-Ras4B HVR was titrated into ^{15}N CaM, shift changes were observed across the C-lobe and the central linker region (39), although they were smaller than those we observed with RalA HVR peptide (*SI Appendix*, Fig. S5). A recent structure of CaM in complex with a farnesylated and carboxymethylated cysteine (FCME) shows that FCME binds the CaM C-lobe (22). This is supported by affinity measurements of the individual lobes of CaM for lipidated K-Ras4B, which showed that the C-lobe binds with a similar affinity to that of full-length CaM (21). In contrast, in the context of the prenylated RalA HVR, we have shown that it is the N-lobe that is responsible for engaging the prenyl moiety. The two hydrophobic anchor residues that we have identified are responsible for "steering" the orientation of the RalA HVR. They contact the C-lobe even in the absence of the farnesyl group, blocking this lobe and forcing the isoprenyl to bind the N-lobe pocket.

Comparison of the farnesyl-binding pockets of the CaM C-lobe and N-lobe (Fig. 4*D*) reveals remarkable similarity in the hydrophobic cavity that buries the prenyl anchor. The prenyl anchor penetrates to the base of the pocket where it interacts with the methyl-containing Ile27^{N}/Ile100^{C} (superscript denotes the CaM lobe), Leu32^{N}/Leu105^{C}, and Ile63^{N}/Val136^{C}. Two equivalent Phe sidechains pack one side of the binding pocket: Phe19^{N}/Phe92^{C} and Phe68^{N}/Phe141^{C}. The entrance to each pocket is lined by two pairs of Met sidechains: Met36^{N}/Met109^{C}, Met51^{N}/Met124^{C} and Met71^{N}/Met144^{C}, Met72^{N}/Met145^{C}. These flexible sidechains allow the prenyl moiety to leave the pocket in two different directions in the two structures (Fig. 4*D*). In the closed structure of CaM in complex with FCME alone (40), the prenyl is clamped by contacts with the N-lobe, which stabilizes one orientation, whereas in the context of RalA, the prenyl anchor exits the hydrophobic cavity in an alternative orientation that allows the RalA HVR to interact with the C-lobe of CaM.

It has been suggested that RalA, RalB, K-Ras4B, Rac1, Cdc42, and Rap1A bind in a similar manner to CaM (40), but in light of the structure presented here it seems that RalA and K-Ras4B bind very differently. Inspection of the sequence of the RalA HVR (Fig. 4*E*) reveals a 1-5-10 spacing of Leu195, Ile199, and GG that is key for both membrane removal and high affinity interaction (Figs. 1*D* and 4*B* and *SI Appendix*, Fig. S9). None of the other CaM-binding GTPases possess this 1-5-10 pattern of

hydrophobic anchor points in their HVR. RalB has a single Phe at position 5 and binds less tightly to CaM (*SI Appendix*, Fig. S12). Indeed, this difference in affinity could drive selection of RalA over RalB at the membrane. This could lead to CaM binding the Ral proteins in different cellular contexts, which may account for some of the functional divergence between these closely related proteins. Rac1 and Rap1A also contain a single hydrophobic residue in their HVRs but with different spacing and it remains to be determined whether the single hydrophobic sidechain is sufficient to drive helix formation and a complex where the farnesyl is bound at the N-lobe. In contrast, K-Ras4B and Cdc42 have only the prenyl lipid as a hydrophobic anchor motif. The absence of a hydrophobic anchor within the HVR, as seen for K-Ras4B, seems to result in a complex where the protein itself is not involved in the interaction with CaM, and only the lipid-modified C-terminal Cys mediates binding. Such an interaction is much weaker and would not be specific, since any isoprenylated protein could bind as long as its C terminus is available in the context of the full-length protein. The K_d of K-Ras4B for bilayers is 4 μM (41), 10-fold weaker than its affinity for CaM. Therefore, the lower affinity of Ras for membranes makes it possible to capture K-Ras4B by binding only to its farnesyl. All the other CaM-binding small G proteins in Fig. 4*E* are geranylgeranylated, which is more hydrophobic (20 versus 15 carbons) and has a higher affinity for the membrane so that the geranylgeranyl would be less available for interaction with CaM. For RalA, we have shown that the initial binding of the hydrophobic anchor residues is required for CaM binding and membrane removal. Cdc42 has no obvious hydrophobic groups that could play this part so that it is not clear whether CaM can bind this protein in the context of a membrane. The role of the single hydrophobic sidechain in the other proteins shown in Fig. 4*E* has not yet been explored. The maleimido-prenyl lipids that we have used in this work could be used to study other GTPases and shed light on the similarities and differences in this class of noncanonical CaM-binding motifs.

In conclusion, this study represents a detailed investigation of the RalA–CaM complex and the first structure of a lipidated HVR–CaM complex. The structure is dynamic due to the intrinsic disorder and flexibility between two hydrophobic modules of the HVR, and CaM removes RalA from its membrane environment. The methods we have employed to study this complex could be used in further research involving CaM and small GTPases and could help shed light on the similarities and differences in these related proteins. From first investigations into the interaction between the complex of CaM and RalB, the closest relative of RalA, there are already hints of differences in these interactions that could underpin the functional divergence between these isoforms.

Materials and Methods

Detailed experimental procedures are described in *SI Appendix*, *Supplementary Materials and Methods*. The different RalA constructs used in the various experiments are shown in *SI Appendix*, Table S1.

NMR Measurements. NMR data were collected at 25 °C using Bruker AV800 and AV950 spectrometers. Data were processed using AZARA and analyzed using Ccpnmr Analysis (42).

ITC Experiments. ITC was performed using a MicroCal iTC200 System (Cytiva), with CaM in the syringe and RalA in the cell. Data were processed in Origin; heats from injection of CaM into buffer were subtracted from the experimentally observed heat changes. Best fits were obtained using the "One Set of Sites" binding model.

SPR Experiments. Experiments were performed on the Biacore T200 system (Cytiva). Experiments to estimate the binding affinity between CaM and Ral constructs were carried out with CaM immobilized to a Series S CM5 chip. Multicycle experiments were carried out with regeneration by stripping the Ca^{2+} from CaM with buffer containing 25 mM EDTA. Membrane experiments were carried out by adapting the protocols in refs. 33 and 43. Liposomes were immobilized on a Series S L1 chip; RalA-MFn was flowed over the membrane surface and washed with buffer before CaM was injected across the surface. Control experiments to confirm membrane coverage, nonspecific RalA binding, and removal were also performed.

Pull-Down Experiments. RalA-MGG on the surface of nanodiscs was bound to Ni-NTA resin, which was washed to remove nonbound protein. Resin was then incubated in buffer containing Ca^{2+}-CaM or buffer alone, which was removed in four elution washes. Samples were run on 15% SDS-PAGE (sodium dodecyl sulphate polyacrylamide gel electrophoresis), before visualization either with Coomassie staining (for CaM) or Western blot to resolve the similarly sized RalA and MSP1D1.

Data Availability. Structure and chemical shifts data have been deposited in the protein data bank (PDB) and Biological Magnetic Resonance Data Bank (7NQC and 34608).

ACKNOWLEDGMENTS. This work was supported by a Biotechnology and Biological Sciences Research Council (BB/P504853/1) and AstraZeneca CASE studentship to H.R.M. and S.G.C. This work was supported by the Francis Crick Institute through provision of access to the Medical Research Council Biomedical NMR Centre. The Francis Crick Institute receives its core funding from Cancer Research UK (FC001029), the UK Medical Research Council (FC001029), and the Wellcome Trust (FC001029). We are grateful to Dr Daniel Nietlispach for his help with acquisition of nonuniform sampled and X-filter NMR experiments and Dr Katherine Stott for her helpful discussions of the ITC data.

1. N. M. Hamad *et al.*, Distinct requirements for Ras oncogenesis in human versus mouse cells. *Genes Dev.* **16**, 2045–2057 (2002).
2. A. Rangarajan, S. J. Hong, A. Gifford, R. A. Weinberg, Species- and cell type-specific requirements for cellular transformation. *Cancer Cell* **6**, 171–183 (2004).
3. J. Yin *et al.*, Activation of the RalGEF/Ral pathway promotes prostate cancer metastasis to bone. *Mol. Cell. Biol.* **27**, 7538–7550 (2007).
4. A. González-García *et al.*, RalGDS is required for tumor formation in a model of skin carcinogenesis. *Cancer Cell* **7**, 219–226 (2005).
5. R. B. Fenwick *et al.*, Solution structure and dynamics of the small GTPase RalB in its active conformation: Significance for effector protein binding. *Biochemistry* **48**, 2192–2206 (2009).
6. K.-H. Lim *et al.*, Activation of RalA is critical for Ras-induced tumorigenesis of human cells. *Cancer Cell* **7**, 533–545 (2005).
7. K.-H. Lim *et al.*, Divergent roles for RalA and RalB in malignant growth of human pancreatic carcinoma cells. *Curr. Biol.* **16**, 2385–2394 (2006).
8. T. D. Martin, C. J. Der, Differential involvement of RalA and RalB in colorectal cancer. *Small GTPases* **3**, 126–130 (2012).
9. N. F. Neel *et al.*, The RalB small GTPase mediates formation of invadopodia through a GTPase-activating protein-independent function of the RalBP1/RLIP76 effector. *Mol. Cell. Biol.* **32**, 1374–1386 (2012).
10. G. Oxford *et al.*, RalA and RalB: Antagonistic relatives in cancer cell migration. *Cancer Res.* **65**, 7111–7120 (2005).
11. J. Cornish, S. G. Chamberlain, D. Owen, H. R. Mott, Intrinsically disordered proteins and membranes: A marriage of convenience for cell signalling? *Biochem. Soc. Trans.* **48**, 2669–2689 (2020).
12. S. Dharmaiah *et al.*, Structural basis of recognition of farnesylated and methylated KRAS4b by PDEδ. *Proc. Natl. Acad. Sci. U.S.A.* **113**, E6766–E6775 (2016).
13. T. S. Reid, K. L. Terry, P. J. Casey, L. S. Beese, Crystallographic analysis of CaaX prenyltransferases complexed with substrates defines rules of protein substrate selectivity. *J. Mol. Biol.* **343**, 417–433 (2004).
14. A. M. Winter-Vann, P. J. Casey, Post-prenylation-processing enzymes as new targets in oncogenesis. *Nat. Rev. Cancer* **5**, 405–412 (2005).
15. K.-H. Lim *et al.*, Aurora-A phosphorylates, activates, and relocalizes the small GTPase RalA. *Mol. Cell. Biol.* **30**, 508–523 (2010).
16. Y. S. Babu, C. E. Bugg, W. J. Cook, Structure of calmodulin refined at 2.2 A resolution. *J. Mol. Biol.* **204**, 191–204 (1988).
17. M. Zhang, T. Tanaka, M. Ikura, Calcium-induced conformational transition revealed by the solution structure of apo calmodulin. *Nat. Struct. Biol.* **2**, 758–767 (1995).
18. M. Zhang, M. Li, J. H. Wang, H. J. Vogel, The effect of Met—>Leu mutations on calmodulin's ability to activate cyclic nucleotide phosphodiesterase. *J. Biol. Chem.* **269**, 15546–15552 (1994).
19. H. Tidow, P. Nissen, Structural diversity of calmodulin binding to its target sites. *FEBS J.* **280**, 5551–5565 (2013).
20. R. R. Clough, R. S. Sidhu, R. P. Bhullar, Calmodulin binds RalA and RalB and is required for the thrombin-induced activation of Ral in human platelets. *J. Biol. Chem.* **277**, 28972–28980 (2002).
21. C. Agamasu *et al.*, KRAS prenylation is required for bivalent binding with calmodulin in a nucleotide-independent manner. *Biophys. J.* **116**, 1049–1063 (2019).
22. B. M. M. Grant *et al.*, Calmodulin disrupts plasma membrane localization of farnesylated KRAS4b by sequestering its lipid moiety. *Sci. Signal.* **13**, eaaz0344 (2020).

23. K. L. Wang, M. T. Khan, B. D. Roufogalis, Identification and characterization of a calmodulin-binding domain in Ral-A, a Ras-related GTP-binding protein purified from human erythrocyte membrane. *J. Biol. Chem.* **272**, 16002–16009 (1997).
24. J.-B. Park, Regulation of GTP-binding state in RalA through Ca^{2+} and calmodulin. *Exp. Mol. Med.* **33**, 54–58 (2001).
25. R. S. Sidhu, S. M. Elsaraj, O. Grujic, R. P. Bhullar, Calmodulin binding to the small GTPase Ral requires isoprenylated Ral. *Biochem. Biophys. Res. Commun.* **336**, 105–109 (2005).
26. S. M. Elsaraj, R. P. Bhullar, Regulation of platelet Rac1 and Cdc42 activation through interaction with calmodulin. *Biochim. Biophys. Acta* **1783**, 770–778 (2008).
27. M. Fivaz, T. Meyer, Reversible intracellular translocation of KRas but not HRas in hippocampal neurons regulated by Ca^{2+}/calmodulin. *J. Cell Biol.* **170**, 429–441 (2005).
28. J.-B. Park, J.-Y. Lee, J.-W. Kim, Dissociation of RalA from synaptic membranes by Ca^{2+}/calmodulin. *Biochem. Biophys. Res. Commun.* **263**, 765–769 (1999).
29. M. Ikura, A. Bax, Isotope-filtered 2D NMR of a protein-peptide complex: Study of a skeletal muscle myosin light chain kinase fragment bound to calmodulin. *J. Am. Chem. Soc.* **114**, 2433–2440 (1992).
30. C. Zwahlen *et al*., Methods for measurement of intermolecular NOEs by multinuclear NMR spectroscopy: Application to a bacteriophage λ N-peptide/boxB RNA complex. *J. Am. Chem. Soc.* **119**, 6711–6721 (1997).
31. E. Krissinel, K. Henrick, Inference of macromolecular assemblies from crystalline state. *J. Mol. Biol.* **372**, 774–797 (2007).
32. C. Lopez-Alcalá *et al*., Identification of essential interacting elements in K-Ras/calmodulin binding and its role in K-Ras localization. *J. Biol. Chem.* **283**, 10621–10631 (2008).
33. B. Sperlich, S. Kapoor, H. Waldmann, R. Winter, K. Weise, Regulation of K-Ras4B membrane binding by calmodulin. *Biophys. J.* **111**, 113–122 (2016).
34. F. Rodríguez-Castañeda *et al*., Modular architecture of Munc13/calmodulin complexes: Dual regulation by Ca^{2+} and possible function in short-term synaptic plasticity. *EMBO J.* **29**, 680–691 (2010).
35. J. Vlach, A. B. Samal, J. S. Saad, Solution structure of calmodulin bound to the binding domain of the HIV-1 matrix protein. *J. Biol. Chem.* **289**, 8697–8705 (2014).
36. M. Nagulapalli *et al*., Recognition pliability is coupled to structural heterogeneity: A calmodulin intrinsically disordered binding region complex. *Structure* **20**, 522–533 (2012).
37. J. E. Taylor *et al*., Calmodulin binds a highly extended HIV-1 MA protein that refolds upon its release. *Biophys. J.* **103**, 541–549 (2012).
38. P. Villalonga *et al*., Calmodulin binds to K-Ras, but not to H- or N-Ras, and modulates its downstream signaling. *Mol. Cell. Biol.* **21**, 7345–7354 (2001).
39. S. J. Abraham, R. P. Nolet, R. J. Calvert, L. M. Anderson, V. Gaponenko, The hypervariable region of K-Ras4B is responsible for its specific interactions with calmodulin. *Biochemistry* **48**, 7575–7583 (2009).
40. B. M. M. Grant, M. Enomoto, M. Ikura, C. B. Marshall, A non-canonical calmodulin target motif comprising a polybasic region and lipidated terminal residue regulates localization. *Int. J. Mol. Sci.* **21**, 2751 (2020).
41. W. K. Gillette *et al*., Farnesylated and methylated KRAS4b: High yield production of protein suitable for biophysical studies of prenylated protein-lipid interactions. *Sci. Rep.* **5**, 15916 (2015).
42. W. F. Vranken *et al*., The CCPN data model for NMR spectroscopy: Development of a software pipeline. *Proteins* **59**, 687–696 (2005).
43. A. Gohlke, G. Triola, H. Waldmann, R. Winter, Influence of the lipid anchor motif of N-ras on the interaction with lipid membranes: A surface plasmon resonance study. *Biophys. J.* **98**, 2226–2235 (2010).